

# High CO/H<sub>2</sub> ratios supports an exocometary origin for a CO-rich debris disk

K.D. Smith<sup>1</sup>                                          <img alt="Check for updates icon" data-bbox="730

spectra by the *Hubble Space Telescope* (*HST*) (eg. Roberge et al. 2000), rotational transitions in emission detectable in mm with ALMA (eg. Matrà et al. 2017b; Cataldi et al. 2023; Rebollido et al. 2022) and IR absorption from rovibrational transitions as detected using the Gemini South Telescope and the NASA Infrared Telescope Facility around  $\beta$  Pictoris (Troutman et al. 2011).

CO emission from rotational transitions observed with ALMA has shown exocometary belts can be separated into 2 categories of: CO-rich ( $M_{\text{CO}} \gtrsim 10^{-3} M_{\oplus}$ ) and CO-poor ( $M_{\text{CO}} \lesssim 10^{-3} M_{\oplus}$ ) (Marino et al. 2020). This bimodal distribution of exocometary CO masses can be seen in Cataldi et al. (2023), with CO masses measured directly through  $^{12}\text{C}^{16}\text{O}$  lines (if optically thin) or through  $^{13}\text{C}^{16}\text{O}$  or  $^{12}\text{C}^{18}\text{O}$  measurements (if optically thick and assuming interstellar isotopologue ratios). This gas could be primordial if persisting from the parent protoplanetary disk (Nakatani et al. 2023; Kóspál et al. 2013) or secondary if produced *in-situ* by outgassing from exocomets (Zuckerman & Song 2012). Emission from OI has also been detected in the far IR by (Riviere-Marichalar et al. 2014).

When determining the origin of the CO observed in exocometary belts, it is important to consider the role of UV shielding, which attenuates UV photons and lengthens the time taken for CO to photodissociate (typical photodissociation timescales can be found in Visser et al. 2009; Heays et al. 2017). Unlike in protoplanetary disks, the dust in exocometary belts is optically thin at all wavelengths (e.g Matrà et al. 2018a). Thus, it cannot provide circumstellar gas with substantial shielding from the UV radiation due to the host star and interstellar radiation field (ISRF).

If the gas is primordial, the abundant  $\text{H}_2$  inherited from the protoplanetary disk could provide shielding (Kóspál et al. 2013). If the gas is secondary, CO can be replenished by outgassing from exocomets in the belt (Zuckerman & Song 2012), and shielding could be provided by CO itself (self-shielding) and/or atomic carbon (Matrà et al. 2017a; Kral et al. 2019), which could be produced by photodissociation of carbon-bearing parent molecules such as CO but also yet unseen species such as  $\text{CO}_2$  and  $\text{CH}_4$ . In CO-poor belts, the main way to distinguish between the primordial and secondary scenarios has so far been to compare the CO photodissociation timescale to the system age, with longer timescales allowing for a primordial origin and shorter implying secondary gas. For CO-rich belts, the origin scenario is unclear but a key signature of primordial gas would be a  $\text{H}_2$  abundance comparable with protoplanetary disks.

UV shielding of CO by self-shielding, CI, and  $\text{H}_2$  has traditionally been thought to be important to the longevity of CO in circumstellar disks. In CO-rich debris disks, it is possible that primordial  $\text{H}_2$  abundance, assumed through a protoplanetary like  $\frac{\text{CO}}{\text{H}_2}$  ratio could shield the gas for a few Myr. However, for CO-poor belts numerous studies show that even assuming generously low  $\frac{\text{CO}}{\text{H}_2}$  ratios of  $10^{-6}$ , provide insufficient shielding for primordial CO to persist to the typically older ages of these systems (e.g Marino et al. 2016; Matrà et al. 2017b; Marino et al. 2018; Matrà et al. 2019; Kral et al. 2019). This implies that gas in CO-poor systems, from younger systems like  $\beta$  Pictoris (Matrà et al. 2017a) to older systems like Fomalhaut (Matrà et al. 2017b) and  $\eta$  Corvi (Marino et al. 2016), is most likely secondary. This was corroborated by upper limits on the  $\text{H}_2$  density in the  $\beta$  Pictoris disk obtained from non-local thermodynamic

equilibrium (non-LTE) modelling of the CO excitation (Matrà et al. 2017a).

In CO-rich belts, on the other hand, the origin of the gas remains an open question. These disks have CO masses comparable with the lower end observed in Herbig-Ae protoplanetary disks around stars that are several Myr to a few 10s of Myr old (Moór et al. 2020). If the gas in these CO-rich disks is primordial, we would expect a large amount of  $\text{H}_2$ , the most abundant molecular species in primordial gas. In protoplanetary disks, the gas phase CO-to- $\text{H}_2$  ratio appears to decrease over time, producing  $\frac{\text{CO}}{\text{H}_2}$  ratios between  $10^{-4}$  and  $10^{-6}$  (see Figure 5, Table D.1 and Bergin & Williams (2018); Zhang et al. (2020)). This is because CO abundances start close to ISM-like, but overtime CO can be processed into other carbon-carriers (such as  $\text{CO}_2$  and  $\text{CH}_3\text{OH}$ ) and at the same time CO can be sequestered onto icy grains as they grow and settle to the mid-plane (Schwarz et al. 2018; Bosman et al. 2018; Krijt et al. 2018, 2020). For comparison, in Solar System comets,  $\frac{\text{CO}}{\text{H}_2}$  ratios as high as 0.73 have been observed as  $\text{H}_2$  is mainly produced as a product of  $\text{H}_2\text{O}$  photodissociation (Bockelée-Morvan & Biver 2017; Feldman et al. 2002). Thus, in exocometary belts, a  $\frac{\text{CO}}{\text{H}_2}$  abundance ratio higher than  $10^{-4}$  is diagnostic of a secondary gas origin and this ratio can be used to calculate whether there is sufficient  $\text{H}_2$  shielding to allow persistence of CO to the ages of these systems without replenishment or other shielding mechanisms.

Some constraints on the presence of  $\text{H}_2$  in exocometary belts are present in the literature. For example, using *HST* Lecavelier des Etangs et al. (2001) constrained upper limits for the column density of  $\text{H}_2$  along the line of sight to the edge-on, CO-poor  $\beta$  Pictoris disk to be  $< 0.1 M_{\oplus}$  and combined this with a CO column density (Roberge et al. 2000) to find a  $\frac{\text{CO}}{\text{H}_2}$  ratio lower limit of  $6 \times 10^{-4}$ , higher than expected of primordial gas. Their conclusion is in agreement with the conclusions of Matrà et al. (2017a) that a primordial origin scenario for the gas in  $\beta$  Pictoris is unlikely as there is insufficient  $\text{H}_2$  present to provide shielding for the lifetime of the system.  $\text{H}_2$  can also be indirectly constrained by gas kinematics/distribution. Fernandez et al. (2005) uses the breaking experienced by ionised metallic gas due to unseen neutral  $\text{H}_2$  gas to estimate the  $\text{H}_2$  mass in  $\beta$  Pictoris. Hughes et al. (2017) uses the scale height of the gas in 49 Ceti to infer an upper limit for  $\text{H}_2$ , *via* the mean molecular weight of the gas required by models to reproduce the observed scale height for CO.

Hot  $\text{H}_2$  emission has also been detected in systems bearing debris disks such as TWA 7 (Flagg et al. 2021) and AU Mic (Flagg et al. 2022), where the latter has no evidence for CO (Cronin-Coltsmann et al. 2023). It is unclear whether this hot  $\text{H}_2$  could originate from star spots or an inner disk of gas accreting onto the star, unrelated to the outer disks. Other works have attempted to detect warm  $\text{H}_2$  with Spitzer, but these observations lacked the SNR/sensitivity to confirm or refute a primordial origin scenario (Chen et al. 2007; Kóspál et al. 2013).

We use the newly upgraded, high-resolution CRIRES+ instrument on the VLT to observe the edge-on, CO-rich disks around HD 110058 and HD 131488. With a spectral resolution  $R \sim 100000$  (Leibundgut et al. 2022), CRIRES+ is ideal for detecting line of sight absorption due to CO and  $\text{H}_2$ . Our observations cover multiple rovibrational lines of  $^{12}\text{CO}$  from the  $v=2-0$  level. Absorption from CO in edge-on debris disks has been successfully observed by Troutman et al. (2011), who reported low- $J$  CO absorption from the  $\beta$  Pictoris disk using IRTF/CSHELL. Worthen et al. (2024) reported a non-detection of CO in absorp-

tion toward the edge-on HD 32297 disk using IRTF/iSHELL which was used to estimate the scale height of the disk and place an upper limit on the line-of-sight CO column density. The two disks in this study were measured in absorption in the UV using *Hubble* by ?. Our CRIRES+ observations allow for CO column density and temperature estimates for both HD 110058 and HD 131488.

In this work, we aim to directly probe the column density of H<sub>2</sub> within CO-rich exocometary belts for the first time, and in doing so establish the CO origin. We expect any exocometary H<sub>2</sub> to be co-located with and similar temperature as the CO detected through UV absorption spectroscopy in both disks by ? and in IR in this work. However it is worth noting that H<sub>2</sub> should have a larger vertical extent than CO due to CO being more readily photodissociated at the disk's surface and it's lower mean molecular weight (Marino et al. 2020; Hughes et al. 2017). Both H<sub>2</sub> and CO should be cold and produce narrow absorption lines from their ground vibrational energy levels. We focus on absorption spectroscopy in edge-on belts to use the star as a bright background continuum, and maximise the column density of gas along the line of sight to it. We identified the H<sub>2</sub> v=1-0 S(0) line at 2223 nm as the most promising transition probing rovibrational absorption from the ground level of the H<sub>2</sub> molecule. This is because, assuming the H<sub>2</sub> gas in these systems has a similar temperature to the CO and is in LTE, this line would be the strongest IR transition.

Stellar and disk properties for HD 110058 and HD 131488 are detailed in Table 1. Both are A-type stars (the most common spectral type for CO-rich belts, Moór et al. 2020) and thus provide bright stellar continua against which we searched for absorption. The disks in these systems are also very close to edge-on with inclinations of  $85.5^{+2.5}_{-7.2} \pm 3^\circ$  respectively (Moór et al. 2017; Hales et al. 2022). We choose these two young ( $\sim 15$  Myr), CO-rich, edge-on belts as they have the highest CO column densities detected in absorption to date (?).

In Section 2 we describe the CRIRES+ observations and data reduction. In Section 3 we describe the modelling of H<sub>2</sub> and <sup>12</sup>CO for the two disks and the resulting constraints on the  $\frac{\text{CO}}{\text{H}_2}$  ratio. In Section 4 we compare this ratio with observations of protoplanetary disks and describe how this impacts our understanding of gas detections in CO-rich exocometary belts. In Section 5 we conclude with a summary of our findings.

## 2. Observations and Data Reduction

### 2.1. CRIRES+ Observations

Using CRIRES+, the high-resolution near infrared spectrograph on the VLT (Dorn et al. 2023), we observed HD 110058 and HD 131488 over two nights each, as detailed in Table 2. We observed in the K-band with the K2148 filter, which has non-contiguous wavelength orders from 1904 nm to 2452 nm. Our observation dates were chosen such that the H<sub>2</sub> v=1-0 S(0) rovibrational absorption line at 2223 nm was shifted away from nearby weak tellurics, mainly arising from atmospheric water as can be seen in Figure A.1. Our observation windows also covered the weaker H<sub>2</sub> v=1-0 Q(1) transition at 2406.6 nm. If detected, this transition could allow us to derive the excitation temperature of the H<sub>2</sub> gas. Also within the range of the data are the v=2-0 bands from <sup>12</sup>CO, <sup>13</sup>CO, and C<sup>18</sup>O. The latter 2 isotopologues will be examined in upcoming work. No attempt was made to shift CO lines in this data away from nearby tellurics, as can be seen in Figure A.2.

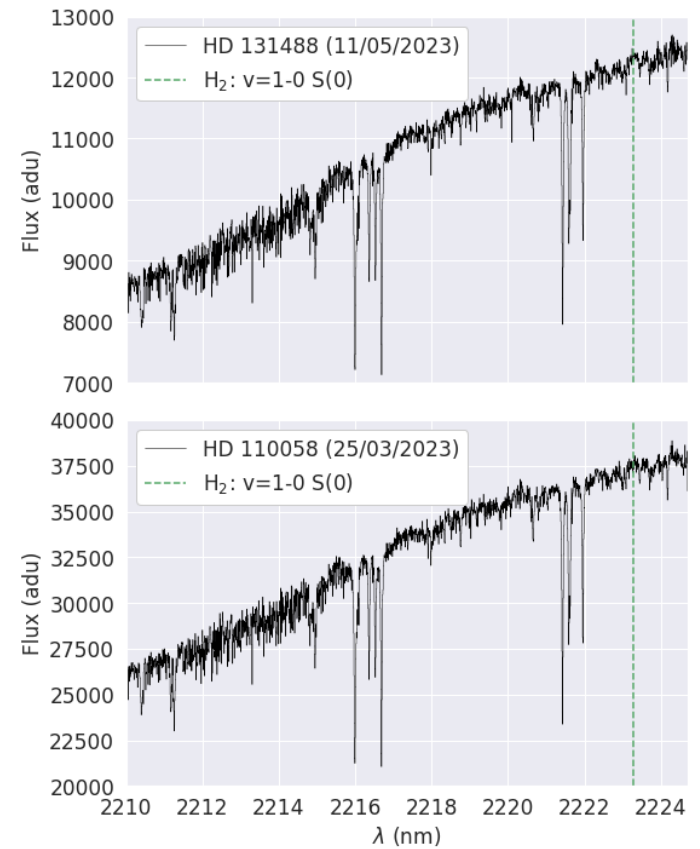


Fig. 1: Reduced and extracted 1D spectra (black lines) for a portion of the detector-order containing our line of interest for HD 131488 on 11/05/23 (top) and HD 110058 on 25/03/23 (bottom). The spectra are not flux calibrated and as such the absolute values of the y-axis in units of analogue-to-digital units (adu) are not astrophysically meaningful. The vertical green line denotes the expected location of the H<sub>2</sub> transition of interest. The spectra are in the observatory frame, but the expected H<sub>2</sub> location has been shifted to the rest frame of the star.

### 2.2. CRIRES+ Data Reduction and Calibration

We used ESOREX and the CR2RES pipeline recipes detailed in the ESO CRIRES+ pipeline user manual (version 1.3.0) to reduce the raw detector images. The standard reduction for nodding observations shown in Figure 4.4 of this manual was the basis of our reduction. High-SNR flats for CRIRES+ are taken once a month, and were used instead of the default supplied flats to improve the final SNR. We performed wavelength calibration with the Uranium-Neon lamp and Fabry-Pérot etalon. After correcting for detector non-linearity, dark current, and then carrying out flat fielding and wavelength calibration, we extracted a 1D spectrum for each of the two nodding positions. A subset of the extracted data (with the two nodding positions combined) covering the wavelength of the H<sub>2</sub> line of interest is shown in Figure 1. This data is yet to be corrected for tellurics or blaze; as such it has arbitrary flux units and displays an upward trend with wavelength.

Our planned analysis required achieving a high-SNR and modelling the line-to-continuum ratio in the continuum normalised spectrum as detailed in Section 3, which made a standard star observation unnecessary. We performed telluric correction using the molecfit software, version 4.3.1 (Smette et al. 2015) which

Table 1: Stellar and Disk Parameters for HD 131488 and HD 110058.

Parameter	HD 131488	References	HD 110058	References
Spectral Type	A1 V	[1]	A0 V	[2]
R.A. (J2000)	14 55 08.03	[1]	12 39 46.14	[2]
Decl. (J2000)	-41 07 13.3	[1]	-49 11 55.84	[2]
K-band Magnitude	7.803	[3]	7.583	[3]
Radial Velocity (km s <sup>-1</sup> )	5.97 <sup>+0.05</sup> <sub>-0.05</sub>	[8]	12.53 <sup>+0.01</sup> <sub>-0.01</sub>	[8]
Distance (pc)	152 <sup>+3.2</sup> <sub>-0.2</sub>	[4]	130 <sup>+2</sup> <sub>-0.2</sub>	[4]
Association	Upper Centaurus Lupus	[1]	Lower Centaurus Crux	[2]
Age	~16 Myr	[1]	~17 Myr	[2]
Log(g)	3.80 <sup>+0.38</sup> <sub>-0.16</sub>	[4]	3.54 <sup>+0.41</sup> <sub>-0.01</sub>	[4]
Stellar Radius (R <sub>⊙</sub> )	1.60 <sup>+0.03</sup> <sub>-0.02</sub>	[4]	1.55 <sup>+0.02</sup> <sub>-0.04</sub>	[4]
Stellar Mass (M <sub>⊙</sub> )	1.8	[5]	1.84	[2]
Disk Inclination (°)	82 <sup>+3</sup> <sub>-3</sub>	[6]	85.5 <sup>+2.5</sup> <sub>-7.2</sub>	[2]
R <sub>in</sub> (au)	35 <sup>+11</sup> <sub>-11</sub>	[7]	7.4 <sup>+2.2</sup> <sub>-7.3</sub>	[2]
R <sub>out</sub> (au)	140 <sup>+11</sup>	[7]	80 ± 12	[2]
log(N <sub>CO</sub> (cm <sup>-2</sup> ))	18.1 <sup>+0.2</sup> <sub>-0.1</sub>	[4]	19.7 <sup>+0.1</sup> <sub>-0.1</sub>	[4]
T <sub>gas</sub> (K)	141 <sup>+103</sup> <sub>-55</sub>	[8]	133.0 <sup>+19</sup> <sub>-18</sub>	[8]

**References.** [1] Melis et al. (2013); [2] Hales et al. (2022); [3] Cutri et al. (2003); [4] ?; [5] Matrà et al. (2018a); [6] Moór et al. (2017); [7] Smirnov-Pinchukov et al. (2022); [8] This work. Note: T<sub>gas</sub> is the kinetic temperature from the <sup>12</sup>CO observations summarised in Appendix C. It is only the same as the kinetic temperature if the system is in LTE and the H<sub>2</sub> is colocated with the CO. R<sub>in</sub> and R<sub>out</sub> are the radii for the CO disk while the disk inclination is derived from the dust disk.

Table 2: Overview of VLT-CRIRES+ observations of HD 110058 and HD 131488.

Target	Programme ID	Night	Exp. time	Obs. mode	Slit	AO loop	Wavelength setting	Airmass
HD 110058	110.248L.001	25/03/2023	12 × 240s	Nodding	0.2"	Closed	K2148	1.134
HD 110058	110.248L.001	08/03/2024	12 × 240s	Nodding	0.2"	Closed	K2148	1.106
HD 131488	111.255A.001	08/05/2023	24 × 120s	Nodding	0.2"	Closed	K2148	1.168
HD 131488	111.255A.001	11/05/2023	24 × 120s	Nodding	0.2"	Closed	K2148	1.122

**Notes.** Note: Exposure time is expressed as number of detector integrations (NDIT) × detector integration time (DIT).

has been shown to perform as well or better than corrections using standard stars on CRIRES data (Ulmer-Moll et al. 2019). We performed telluric correction and telluric-based wavelength calibration on subsets of the data around lines of interest. For more detail see Appendix A and B. Figures A.1 and A.2 show example spectra with telluric fits with the most prominent, yet relatively weak tellurics arising from atmospheric water, while corrected spectra are shown in Figures 2, 3, and 4. We note that, by design, the H<sub>2</sub> line under investigation does not overlap with any telluric lines, thus the removal of tellurics does not significantly affect the spectrum at or near the line. Telluric removal was also carried out for each nodding position/observing day combination for the <sup>12</sup>CO lines in spectral regions covering the v=2-0 rovibrational band from 2318.9 to 2333.9 nm and 2335.455 to 2350.0 nm and for the H<sub>2</sub> v=1-0 S(0) line from 2220 to 2224.5 nm. The nodding positions were modelled separately to allow for improved wavelength calibration described in Appendix B. An advantage of using molecfit is that in addition to telluric removal, it also returns a spectral resolution for the observations, specific to each detector-order, nodding position and observing day combination.

The average resolution over each spectrum in the region corrected by molecfit near the H<sub>2</sub> line, was measured to be R = 126000 ± 9000 for HD 131488 and R = 130000 ± 7000 for HD 110058. For the regions containing the <sup>12</sup>CO, the resolution was measured to be R = 115000 ± 9000 and R = 121000 ± 9000 for HD 131488 and HD 110058 respectively. The resolution varies with the spectral region under consideration, and the weather.

CRIRES+ typically has a resolution of 100000, but because the stars did not fill the slit width, we are in the superresolution regime described in Appendix B. This leads to offsets in wavelength between nodding positions. Thus, we did not use the final CRIRES nodding corrected spectra. Instead we telluric corrected the spectra for each nodding position separately and used the tellurics to ensure each spectrum was correctly wavelength calibrated before modelling.

To identify the H<sub>2</sub> and CO lines at their rest frequencies, the reduced, telluric free spectra for each observing night were Doppler shifted to the rest frame of the star using the systemic and barycentric velocities. The barycentric velocity correction is calculated using Astropy’s SkyCoord class (Collaboration et al. 2022), whereas radial (systemic) velocities for each system were determined through modelling <sup>12</sup>CO in the CRIRES+ data (see Section 3 and Table 1). The spectra molecfit returns are telluric-corrected but not continuum-normalised. We divide the telluric-corrected spectrum with a running median with a large window size to produce continuum normalised spectra.

Our final normalised spectra are heteroscedastic, as across each order the flux of the star changes, and telluric correction produces regions of higher/lower variance. To calculate the variance and therefore an uncertainty per pixel empirically, we therefore masked regions around the CO and H<sub>2</sub> lines of interest and calculated rolling variances with a 20-pixel-wide window, chosen to best capture local variations in variance around the target lines. For the masked pixel locations around these lines, we then lin-

early interpolated the variance from neighbouring pixel regions. The final products used for modelling are 4 spectra of normalised intensity and their empirically-determined uncertainty per target, one for each of two nodding positions and two observing dates. We then median averaged the nods and dates to produce the spectra in Figures 2, 3, and 4.

### 3. Results and Modelling

The final normalised spectra for each star are displayed in Figures 2, 3, and 4, with wavelengths in the rest frame of the star. For H<sub>2</sub>, if detectable, we expect circumstellar gas to produce an absorption line at the v=1-0 S(0) transition wavelength of 2223.29 nm (from the HITRAN database, Gordon et al. 2022). No statistically significant detection of H<sub>2</sub> was found for either system. Additionally, as expected for cold H<sub>2</sub> where the ground state should be the most populated energy level, the weaker 2406.6 nm absorption line arising from the H<sub>2</sub> v=1-0 Q(1) transition was not detected.

For both disks, we detect <sup>12</sup>CO absorption at a radial velocity consistent with that observed in the UV for HD 110058 by ?. The radial velocity for HD 131488 differs from the one reported in ?, but it is consistent with the CO radial velocity observed in emission with ALMA by Mac Manamon (in press) as part of the ARKS program. For HD 110058, we detect the v=2-0, J=15-14 to J=1-0 and for HD 131488 we detect the v=2-0, J=8-7 to J=1-0 transitions. More CO is present in HD 110058, and thus the absorption lines are deeper, reflected in the axis scaling of Figures 3 and 4. Additionally, the excitation temperature for HD 110058 is higher, allowing more high-J transitions to be populated.

#### 3.1. Modelling the Reduced CRIRES+ Spectra

We modelled H<sub>2</sub> absorption in the normalised spectra using RADIS (Pannier & Laux 2019). RADIS relies on the HITRAN line list (Gordon et al. 2022) obtained using the HITRAN Application Programming Interface (Kochanov et al. 2016), and partition functions described in Gamache et al. (2021). Given the non-detection, for H<sub>2</sub> we assumed the gas is in LTE and that it can be approximated as having a single column density and temperature along the line of sight to the star. On the other hand, for CO we found LTE not to be a sufficiently good description of the data and we therefore adopted a simplified non-LTE with a different kinetic temperature (setting the intrinsic line width through Doppler broadening) from the excitation temperature (setting the ratio of the populations of the various rotational levels, and therefore the relative strength of our detected lines). This is consistent with the findings and the modelling of UV rovibronic lines in the same systems (?). Although we cannot determine whether H<sub>2</sub> is in LTE without more information about the collider densities, the H<sub>2</sub> (v=1-0 S(0)) transition has an Einstein A of  $2.524 \times 10^{-7} \text{ s}^{-1}$  while the CO <sup>12</sup>CO  $v = 2 \rightarrow 0$  transitions have Einstein A coefficients on the order of  $10^{-1} \text{ s}^{-1}$ . Meanwhile the collisional rate coefficients found in Thi et al. (2013); Quéméner & Balakrishnan (2009) are of comparable orders of magnitude. This means the H<sub>2</sub> transition has a lower critical density and is therefore more likely to be in LTE than the detected CO.

For a fixed wavelength range RADIS produces a normalised absorption spectrum dependent on temperature (excitation and/or kinetic) and column density, and accounting for optical depth effects. The model spectra are convolved with a Gaussian with

a FWHM equal to the spectral resolution of our observations found using the best-fit models from molecfit. A radial velocity shift was also left as a free parameter. This gives us a final convolved, normalised absorption model for the CO and H<sub>2</sub> rovibrational transitions for any combination of kinetic/excitation temperature, column density, and radial velocity which can be compared with our normalised spectra for each star.

We assessed the goodness of fit for each pair of model parameters with a log Gaussian likelihood ( $\ln \mathcal{L}$ ) function:

$$\ln \mathcal{L} = -\frac{1}{2} \sum_{i=0}^n \frac{(R_i)^2}{\sigma_i^2} + \ln(2\pi\sigma_i^2) \quad (1)$$

where  $R_i$  are the residuals for the  $i^{\text{th}}$  spectral pixel in the normalised spectrum. The uncertainties ( $\sigma_i$ ) for the  $i^{\text{th}}$  pixel are derived empirically as described in Section 2.2.

We use a Markov-Chain Monte Carlo (MCMC) method implemented in python's emcee package (Foreman-Mackey et al. 2013) to sample the posterior probability distribution. We used uniform priors for each parameter and ran the MCMC for 50000 steps with 100 walkers to ensure convergence and to obtain a representative posterior distribution.

#### 3.2. Results

The posterior probability distributions from the MCMC fit are shown in Figures C.1, C.2, C.3, and C.4. There is clear degeneracy between the H<sub>2</sub> temperature and column density which it is not possible to break with a non-detection. For larger temperatures, larger column densities are allowed as fewer H<sub>2</sub> molecules are in the ground state energy level and thus fewer potential absorbers lie between the star and the observer. When marginalised over temperature, we obtain a column density upper limit. The column density posterior is close to a uniform distribution for low column densities as small amounts of H<sub>2</sub> would all equally result in signals below the noise level of the data. Larger column densities would produce larger signals reaching detectability and thus these models are less likely to describe our observations.

<sup>12</sup>CO was detected in both systems as shown in Figure 3 and 4. We used the same modelling approach as H<sub>2</sub>, but the detection of the CO band allows us to constrain more parameters, including the radial velocity which is not constrained for H<sub>2</sub> but is used to create Figure 2 with the expected position of the H<sub>2</sub> line.

The best-fit <sup>12</sup>CO models for each star are shown in Figure C.3 and C.4. Both systems have column densities and excitation temperatures that are well constrained and consistent with those found by ?. Our kinetic temperatures are less well constrained given the lines are individually unresolved or at best marginally resolved. The best-fit values are consistent with the more constraining UV results at the  $3\sigma$  level. The excitation temperatures we derive through MCMC fits (see Figures C.3 and C.4) are consistent with those derived in the UV by ?. The lines are narrow, as expected from cold gas and, on a per-line basis, they are consistent with being spectrally unresolved or at best marginally resolved given the spectral resolution estimated from our telluric fit.

The best-fit parameters for CO are shown in Figures C.3 and C.4 and the best-fit model/residuals are shown in Figures 3 and 4. The posterior distributions in Appendix C indicate that the column densities are constrained by the model. We find that

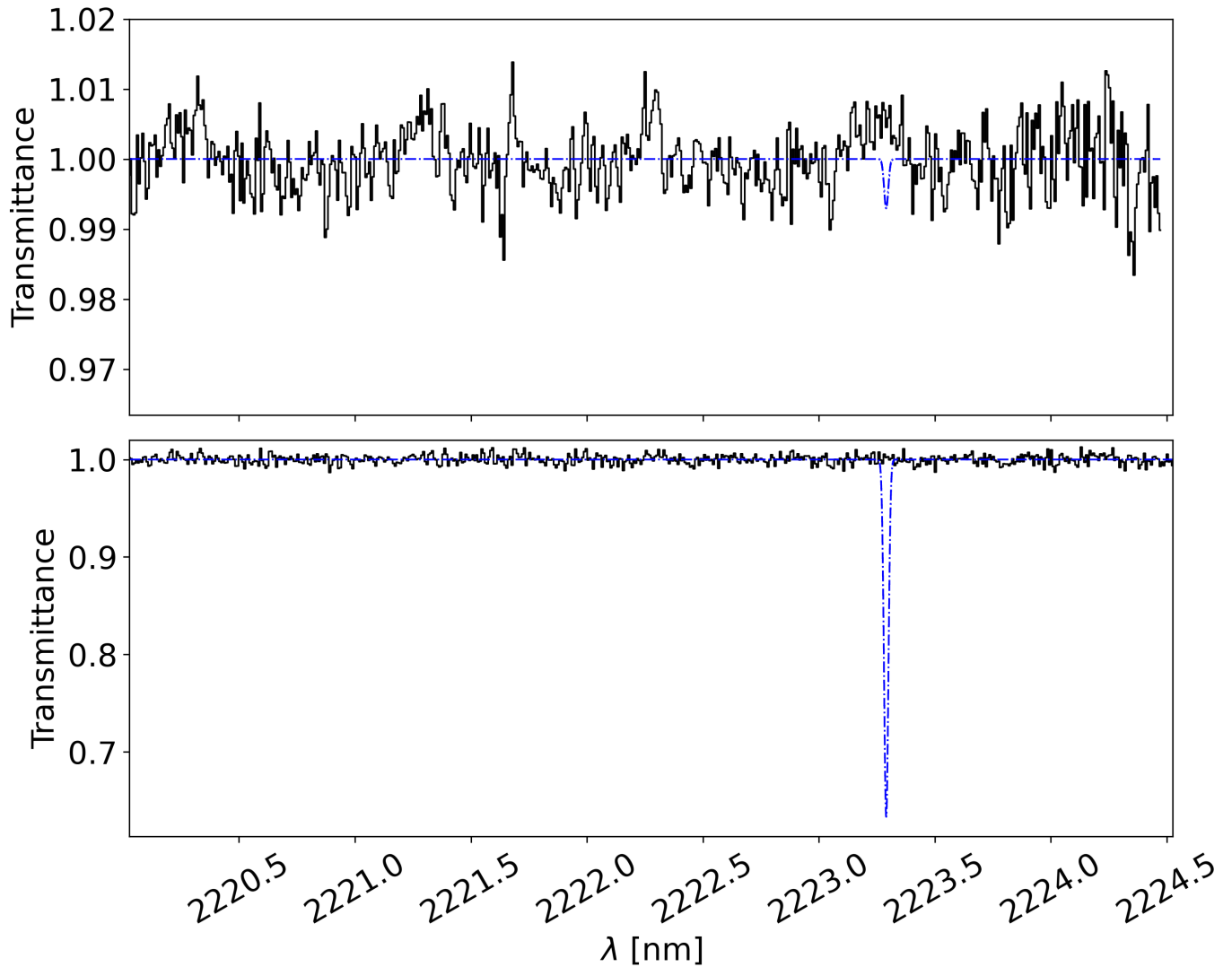


Fig. 2: In black are the median, telluric corrected, normalised spectra of HD 131488 (top) and HD 110058 (bottom). In blue is a model of the  $\text{H}_2$   $v=1-0$   $S(0)$  line assuming a temperature corresponding to the CO kinetic temperature we derive from our results and an  $\text{H}_2$  column density corresponding to an ISM-like, primordial  $\frac{\text{CO}}{\text{H}_2}$  ratio of  $10^{-4}$ .

our best-fit models are very good at representing the data, with some  $3\sigma$  residuals around some optically thick CO lines in HD 110058 as shown in Figures 3 and 4. These small residuals could be due to imperfect telluric correction, and/or the assumed perfectly Gaussian shape of the instrumental spectral response, and/or model assumptions such as the assumption that the line of sight CO column can be represented by one temperature and likely don't meaningfully impact our conclusions.

We present  $\text{H}_2$  column density upper limits without assuming any temperature for the gas in Table D.1. However, to calculate the  $\frac{\text{CO}}{\text{H}_2}$  ratios, we assume that the  $\text{H}_2$  shares the same temperature as the CO kinetic temperature derived from our observations, which is reasonable if CO and any hypothetical  $\text{H}_2$  are co-located. The choice of kinetic rather than excitation temperatures is conservative with regards to how much unseen  $\text{H}_2$  could be present as the colder excitation temperatures derived for CO would lead to lower column densities.

Given the  $\text{H}_2$  column density upper limit, and the CO detection, we can combine their column densities to derive a  $\frac{\text{CO}}{\text{H}_2}$  ratio lower

Table 3: CRIRES+  $\text{H}_2$  data forward modelling results.

	HD 131488	HD 110058
$\log(\text{N}_{\text{CO}} \text{ (cm}^{-2}\text{)})$	$18.05^{+0.06}_{-0.04}$	$19.97^{+0.27}_{-0.20}$
$\log(\text{N}_{\text{H}_2} \text{ (cm}^{-2}\text{)})$	$<22.55$	$<22.84$
CO/ $\text{H}_2$ Ratio	$>3.09 \times 10^{-5}$	$>1.35 \times 10^{-3}$

limit for the gas in both systems. As the column densities for both  $\text{H}_2$  and CO are correlated with the gas temperatures, we first sampled from the CO and  $\text{H}_2$  posterior column density distributions at the same (kinetic) temperature, resulting in a large number of  $\frac{\text{CO}}{\text{H}_2}$  samples representing the  $\frac{\text{CO}}{\text{H}_2}$  probability distribution given our data. We then took the 99.7<sup>th</sup> percentile of this distribution as the  $3\sigma$  lower limit for each system, reported in Tables 3 and D.1.

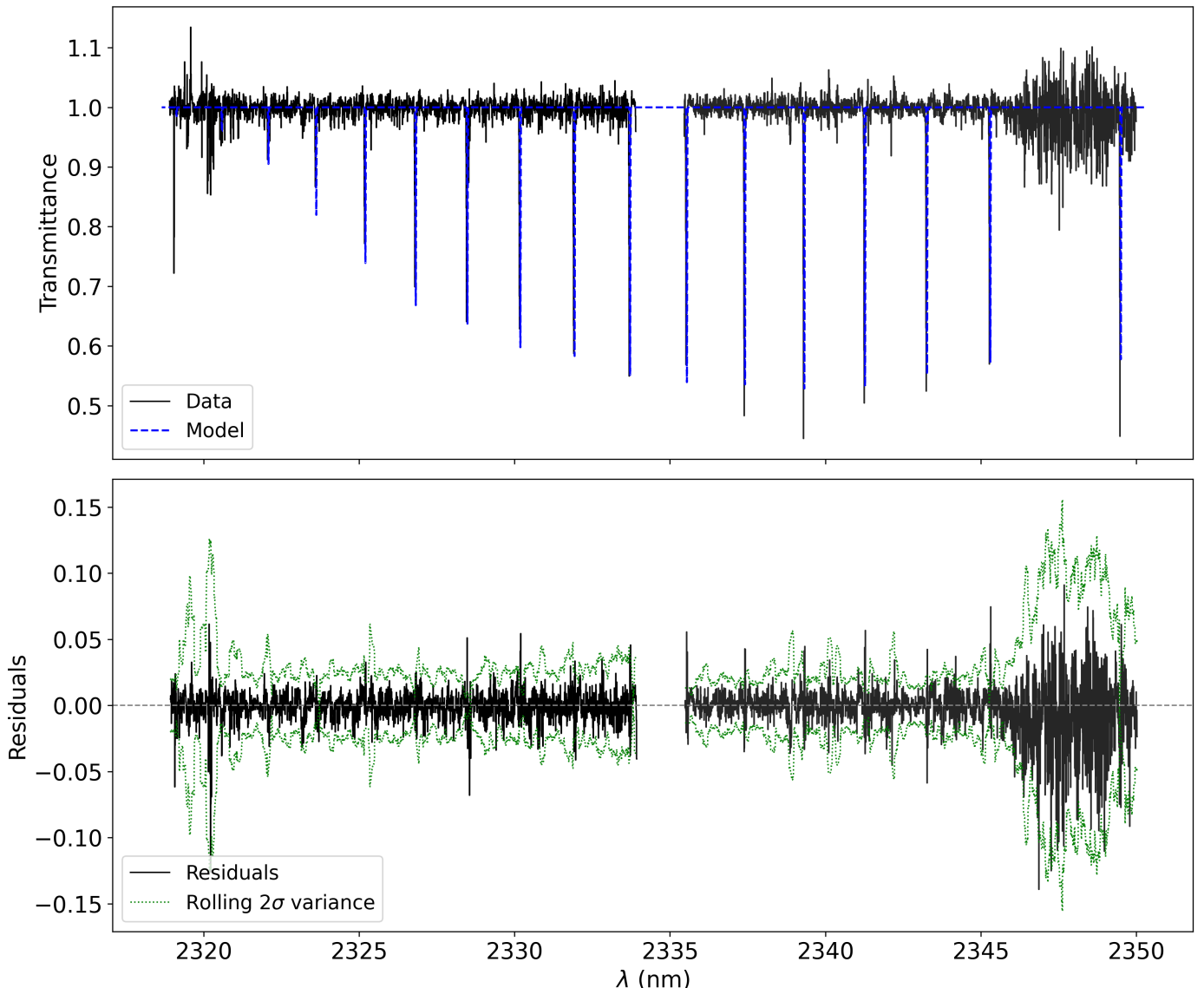


Fig. 3: The top figure shows the HD 110058  $^{12}\text{CO}$  data (black solid line) overlaid with the best-fit model (blue dotted line). The bottom figure shows the  $^{12}\text{CO}$  residuals (black solid line) and the rolling variance (green dashed line).

## 4. Discussion

### 4.1. CO/H<sub>2</sub> ratios across planet formation: CO depletion to enhancement from protoplanetary to debris disks

In the previous sections we presented CRIRES+ observations of the stars HD 110058 and HD 131488, which both host edge-on CO-rich exocometary belts. We detected  $^{12}\text{CO}$  rovibrational absorption from the  $v=2-0$  band, and attempted to detect H<sub>2</sub> in these systems through its rovibrational  $v=1-0$  S(0) line, arising from absorption of cold molecules in the ground state. Despite the high-SNR achieved on the stars with CRIRES+, and the clear CO detections, we do not detect H<sub>2</sub> in either system. To set stringent constraints on its presence, we modelled CO and H<sub>2</sub> absorption using the line-by-line spectral modelling tool RADIS to obtain CO column densities and an H<sub>2</sub> column density upper limit. Combined, these yielded  $\frac{\text{CO}}{\text{H}_2}$  ratio lower limits of  $3.09 \times 10^{-5}$  and  $1.35 \times 10^{-3}$  for HD 131488 and HD 110058 respectively.

We compare our lower limit for the  $\frac{\text{CO}}{\text{H}_2}$  ratio in the exocometary belts' gas to values derived for protoplanetary disks listed in Table D.1 and plotted in Figure 5. Protoplanetary ratios typically range from  $10^{-4}$  to  $10^{-6}$  and tend to drop over time within the first 10 Myr of a star's lifetime (Favre et al. 2013; Kama et al. 2016; McClure et al. 2016; Schwarz et al. 2016; Trapman et al. 2017; Zhang et al. 2017; Bergin & Williams 2018; Zhang et al. 2020). This is in contrast with our first direct measurements (lower limits) for the exocometary belt of HD 110058 which has markedly elevated  $\frac{\text{CO}}{\text{H}_2}$  indicating a much more H<sub>2</sub>-poor environment compared with primordial gas in protoplanetary disks (Bergin & Williams 2018; Zhang et al. 2020). The conservative lower limit we obtained via modelling the H<sub>2</sub> non-detections in the CRIRES+ K-band spectra of HD 110058 is a factor of 13 larger than the canonical  $\frac{\text{CO}}{\text{H}_2}$  ratio of  $10^{-4}$  typical of the ISM, and higher than the lower limit on  $\beta$  Pictoris. For our other target HD 131488, the lower limit still formally allows (albeit at low probability) a primordial  $\frac{\text{CO}}{\text{H}_2}$  ratio similar to that of the ISM and protoplanetary disks.

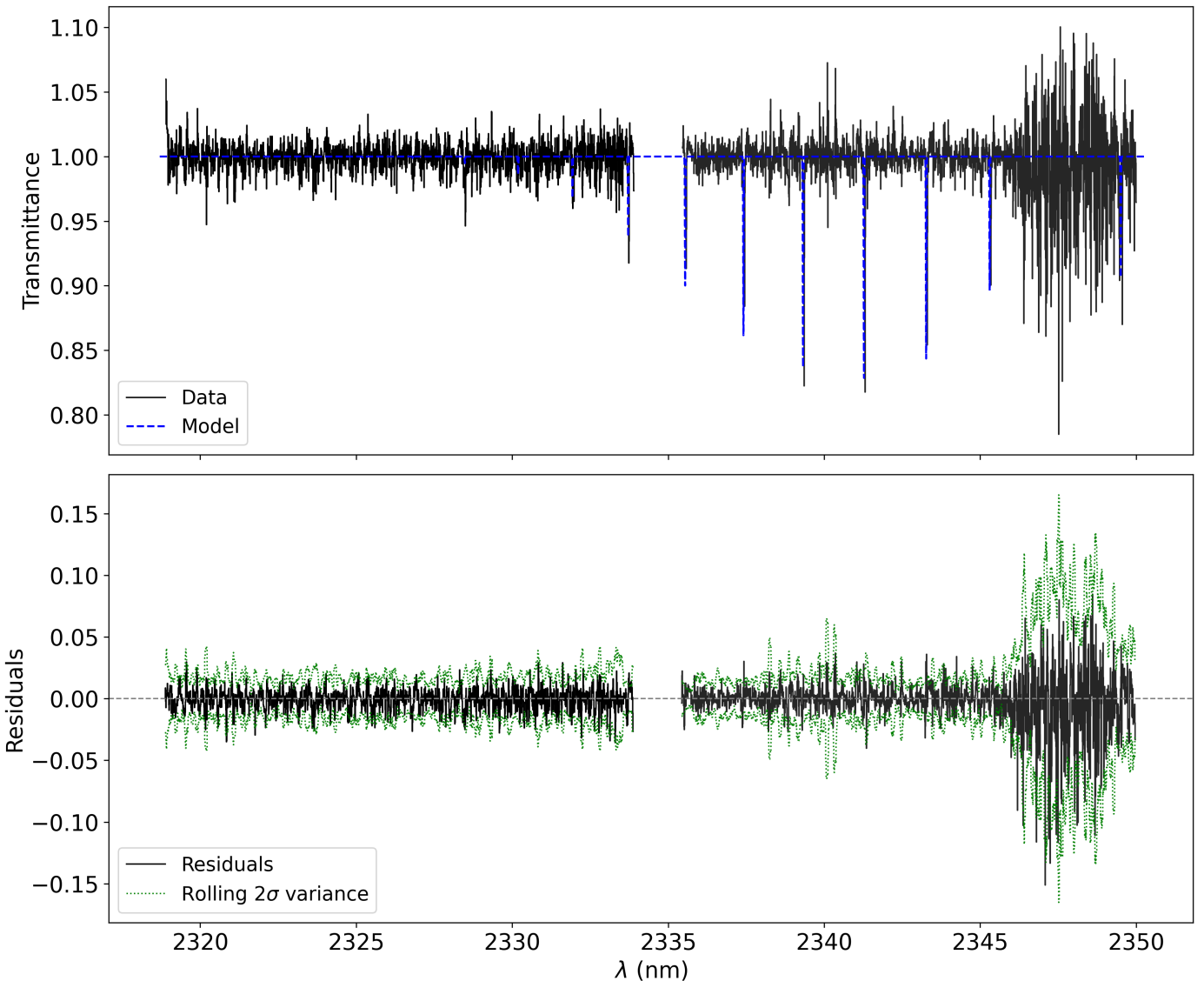


Fig. 4: The top figure shows the HD 131488  $^{12}\text{CO}$  data (black solid line) overlaid with the best-fit model (blue dotted line). The bottom figure shows the  $^{12}\text{CO}$  residuals (black solid line) and the rolling variance (green dashed line).

#### 4.2. $\text{H}_2$ + self-shielding of CO: likely insufficient in a primordial scenario

As discussed in Section 1, another potential way to discriminate between primordial and secondary origin scenarios has been to compare the CO photodissociation timescale to the age of the system, and in particular to evaluate the potential for CO to be shielded from UV radiation. Similar to Marino et al. (2016, 2018); Matrà et al. (2017b, 2019); ? we used half our observationally determined line-of-sight column densities of CO and ( $3\sigma$  upper limit for)  $\text{H}_2$  to calculate shielding factors (Visser et al. 2009) for a CO molecule in the middle of the disk, along the radial direction. In turn, this leads to photodissociation timescales for CO in HD 110058 and HD 131488 of 174 Myr and 61 Myr (respectively) due to ISRF photons.

These give us a likely overly conservative estimate for both systems, not only because these are based on a  $3\sigma$  upper limit, but due to other assumptions. First, ISRF photons can penetrate to the disk midplane much more readily in the vertical direction, because ALMA CO images show the disks to be vertically thin

(Moór et al. 2017; Hales et al. 2022). Shielding factors are a steep function of CO and  $\text{H}_2$  column density; a factor of just a few lower column densities in the vertical direction would shorten the timescale to much less than the system age, rendering shielding much less effective. Second, we only take into account the interstellar radiation field, thus neglecting UV radiation from the host star; if significant, this would further shorten the photodissociation timescale.

We have also taken other assumptions such as that the CO and  $\text{H}_2$  column densities measured by CRIRES+ are representative of the disk midplane, although both disks' inclinations are not perfectly edge-on (Table 1). This is reasonable given that the CO in both disks peaks relatively close to the star in both systems; for example HD 131488 has a CO inner edge  $\lesssim 5$  AU and is vertically resolved in recent high-resolution ALMA data from the ARKS large program (Mac Manamion et al. in press). Finally, our calculation assumes the photodissociation lifetime is representative of the survival times of CO molecules in the disk in the absence of other destruction/production mechanisms,

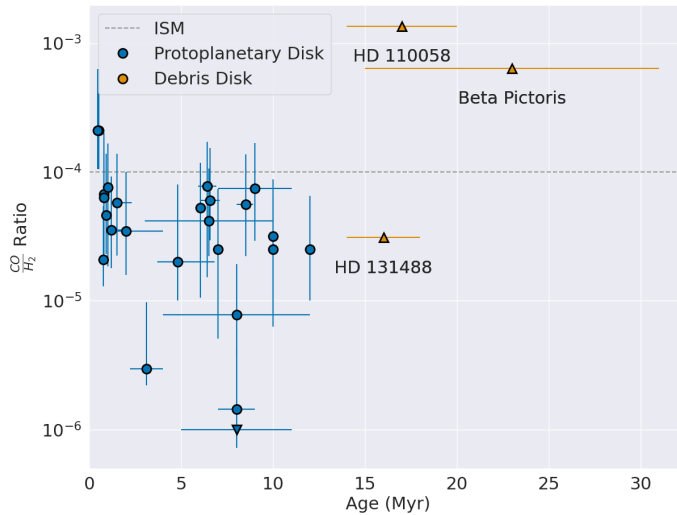


Fig. 5: Ratio of CO and H<sub>2</sub> abundances for protoplanetary disks,  $\beta$  Pictoris, and the two exocometary belts in this study. Details of each point can be found in the references of Table D.1. This plot has been adapted from and expanded upon using the similar plots in Bergin & Williams (2018); Zhang et al. (2020).

such as gas-phase chemistry reforming CO from other species. However, this is only expected to be important in H<sub>2</sub>-rich environments (Higuchi et al. 2017; Iwasaki et al. 2023), which is unlikely to be the case here given our stringent H<sub>2</sub> upper limits.

Overall, most of these assumptions imply that our CO shielding effect and in turn photodissociation timescales in the two systems, calculated from our line of sight column densities of CO and H<sub>2</sub>, are likely significantly overestimated. This could imply that contrary to the values we report, H<sub>2</sub> is likely not able to provide sufficient shielding and allow CO to survive over the lifetime (age) of the systems. This would provide further support to the claim that the gas is not primordial but of second generation in these systems, adding to the new conclusive evidence presented here that the CO/H<sub>2</sub> ratio differs significantly from protoplanetary disk gas in at least one of our two CO-rich systems. Nonetheless, accurately modelling the disk geometry, local radiation field, shielding from various molecules, outgassing rates, etc. would need to be conducted to determine a more realistic photodissociation timescale.

Although CI shielding has not been considered previously in the context of a primordial scenario it could extend the CO lifespan, though it is unclear how important this is in younger protoplanetary disks where complex chemistry beyond simply photodissociation involving both CO and C is expected. What we find is that in the radial direction the CI column density in ? is sufficient to provide shielding over the system lifetime, but it is unclear whether this is possible along the vertical direction as well, where the column density is unconstrained.

For both disks, it also is in principle possible that the belts host a hybrid mix of primordial and secondary gas, with their protoplanetary gas having started to dissipate very recently, as suggested by Lisse et al. (2017). However, our evidence suggests that even in such a scenario, the disks are likely still dominated by second generation gas. Our non-detection of H<sub>2</sub> in both systems is consistent with abundance ratios found in Solar System comets (Combi 1996); supporting the hypothesis that the gas in

these CO-rich systems is, like the dust, secondary/exocometary in origin rather than primordial.

Given the conservative nature of our calculation, even though our photodissociation timescale is older than the age of the system, it is unlikely that any unseen H<sub>2</sub> is sufficient to provide adequate shielding to the CO gas on its own for HD 131488. This is not conclusive evidence against a primordial origin scenario and more complete modelling would need to be conducted to determine a more realistic photodissociation timescale. However, for HD 110058, the CO/H<sub>2</sub> ratio still conclusively rules out that the gas has a primordial-like composition.

#### 4.3. Challenges remain for the second-generation model

While our results strongly point to a secondary origin for the gas at least for HD 110058, challenges remain for modelling secondary gas production and survivability in exocometary belts. Producing the observed column densities in CO-rich belts through exocometary release without shielding may require unreasonably large gas release rates to counter the destruction timescale of unshielded CO, which is  $\sim 130$  years in the ISRF (Heays et al. 2017). To produce the CO mass of  $4 - 8 \times 10^{-2} M_{\oplus}$  found in HD 21997 for example, Kóspál et al. (2013) estimates that approximately 6000 Hale-Bopp sized comets would need to be destroyed yearly. CI (as produced through CO photodissociation) has been posited as a shielding agent to allow for a slower CO release rate and longer accumulation timescales (Matrà et al. 2017a; Marino et al. 2020).

However, ? detected both CO and CI in absorption in the same two systems as this study, finding that the observed column densities of CI are much lower than predicted by the exocometary release model of Marino et al. (2020) and do not provide sufficient shielding for CO. A similar conclusion was reached by Cataldi et al. (2023), who also determined for 14 exocometary belts that the model of Marino et al. (2020) over predicts the amount of CI. These two results suggest that either some of the assumptions are incorrect, the second generation model lacks some important physics/chemistry, or that the gas is primordial; our work deems the latter option to be unlikely. In conclusion, while our results provide the first direct evidence for likely insufficient amounts of H<sub>2</sub> in CO-rich planetesimal belts to shield CO and a markedly different composition to primordial gas in at least one system, current models of second-generation gas release are not yet able to provide a fully self-consistent explanation, and more modelling work and compositional constraints are needed.

Indeed, the molecular composition of gas in CO-rich exocometary belts also remains an open question. Constraints for the presence of molecules have been placed on  $\beta$  Pictoris (Matrà et al. 2018b), 49 Ceti (Klusmeyer et al. 2021), HD 21997, HD 121617, HD 131488, and HD 131835 (Smirnov-Pinchukov et al. 2022). The upper limits found for molecular species in these works differ from the younger protoplanetary disks for which similar searches have been conducted (Smirnov-Pinchukov et al. 2022). The limits are consistent with the secondary generation scenario (Matrà et al. 2018b) but in the case of CN indicate that CO could be preferentially shielded compared to other molecules (Klusmeyer et al. 2021). Higher signal-to-noise ratio observations are likely needed to find molecules other than CO in gas rich exocometary belts. This unprecedented deep search for molecular hydrogen demonstrates the usefulness of IR instruments like CRIRES+ for constraining the composition of ex-

oocometary gas in edge-on exocometary belts. In particular, if the gas is exocometary as strongly supported by our H<sub>2</sub> constraints, observations of IR lines in absorption and mm lines in emission can be used to probe the molecular, volatile content of exocometary material. This is of interest for systems such as HD 131488 and HD 110058 which are a few 10s of Myrs-old and are therefore in the latest stages of terrestrial planet formation when volatile delivery is most likely to occur (Morbidelli et al. 2012, and references therein).

## 5. Conclusions

In this work, we presented CRIRES+ spectra of the edge-on exocometary belts around the  $\sim$ 15 Myr-old A stars HD 131488 and HD 110058. We searched for the H<sub>2</sub> v=1-0 S(0) rovibrational absorption line at 2223 nm and the <sup>12</sup>CO v=2-0 rovibrational band originating from the ground state of the molecule and therefore probed for cold H<sub>2</sub>/CO gas within the exocometary belts, along the line of sight to the central stars. We report the following findings:

- We report detections of the <sup>12</sup>CO v=2-0 rovibrational transitions in HD 131488 and HD 110058 and calculate best-fit, line of sight column densities of 18.05 cm<sup>-2</sup> and 19.97 cm<sup>-2</sup> respectively. We find broad agreement with previous UV observations with *HST* of these disks, with the exception of the kinetic temperatures, which is likely due to the lines being spectrally unresolved, and the radial velocity of HD 131488, although our radial velocity is consistent with mm observations with ALMA.
- We do not detect absorption from the ground state of the H<sub>2</sub> molecule. Modelling this non-detection we calculated upper limits on the H<sub>2</sub> line-of-sight column density of  $< 10^{22.55}$  cm<sup>-2</sup> for HD 131488 and  $< 10^{22.84}$  cm<sup>-2</sup> for HD 110058.
- Combined with our CO detections, we compare the  $\frac{CO}{H_2}$  ratio lower limits of  $3.09 \times 10^{-5}$  (HD 131488) and  $1.35 \times 10^{-3}$  (HD 110058) with protoplanetary disks and conclude that the composition of HD 110058 is significantly different to primordial gas found in protoplanetary disks while that of HD 131488 remains potentially consistent with younger disks at low probability. Further observations would be needed to confirm whether HD 131488 has a primordial or secondary composition.
- H<sub>2</sub> column densities are unlikely to provide sufficient shielding for CO to survive for the system age for both systems. This is because while a very conservative radial estimate leads to timescales of 174 Myr and 61 Myr for HD 110058 and HD 131488, these values are likely orders of magnitude lower when accounting for photodissociation in the vertical direction and by stellar photons.
- Together, these lines of evidence imply that the gas observed in these CO-rich disks is likely second generation gas released by exocomets in the disk, rather than primordial gas leftover from their parent protoplanetary disks.

**Acknowledgements.** KDS and LM acknowledge and thank the Irish research Council (IRC) for funding this work under grant number IRCLA-2022-3788 and the European Union through the E-BEANS project (grant number 100117693). This research used observations made with the European Southern Observatory's CRIRES+ instrument on UT3 of the Very Large Telescope as part of Program ID 111.255A.001. We would like to thank Carlo Manara and the ESO User Support team for their help reducing this data. A. M. H. acknowledges support from the National Science Foundation under Grant No. AST-2307920. AB acknowledges research support by the Irish Research Council under grant GOIPG/2022/1895.

## Data Availability

The observations detailed in this publication are publicly available in the ESO Science Archive Facility (<http://archive.eso.org>) under the program ID 111.255A.001. Data products will be shared on reasonable request to the corresponding author.

## References

Anderson, D. E., Blake, G. A., Bergin, E. A., et al. 2019, The Astrophysical Journal, 881, 127, publisher: The American Astronomical Society

Andrews, S. M., Wilner, D. J., Hughes, A. M., Qi, C., & Dullemond, C. P. 2009, The Astrophysical Journal, 700, 1502, publisher: The American Astronomical Society

Artur de la Villarmois, E., Kristensen, L. E., Jørgensen, J. K., et al. 2018, Astronomy and Astrophysics, 614, A26, aDS Bibcode: 2018A&A...614A..26A

Asensio-Torres, R., Henning, T., Cantalloube, F., et al. 2021, Astronomy and Astrophysics, 652, A101, publisher: EDP ADS Bibcode: 2021A&A...652A.101A

Backman, D. E. & Paresce, F. 1993, Main-Sequence Stars with Circumstellar Solid Material - the VEGA Phenomenon, conference Name: Protostars and Planets III Pages: 1253 ADS Bibcode: 1993prpl.conf.1253B

Bergin, E. A. & Williams, J. P. 2018, The determination of protoplanetary disk masses, publication Title: arXiv e-prints ADS Bibcode: 2018arXiv180709631B

Bockelée-Morvan, D. & Biver, N. 2017, Philosophical Transactions of the Royal Society of London Series A, 375, 20160252, aDS Bibcode: 2017RSPTA.37560252B

Bosman, A. D., Walsh, C., & van Dishoeck, E. F. 2018, Astronomy and Astrophysics, 618, A182, publisher: EDP ADS Bibcode: 2018A&A...618A.182B

Bruderer, S., Dishoeck, E. F. v., Doty, S. D., & Herczeg, G. J. 2012, Astronomy & Astrophysics, 541, A91, publisher: EDP Sciences

Cataldi, G., Aikawa, Y., Iwasaki, K., et al. 2023, The Astrophysical Journal, 951, 111, aDS Bibcode: 2023ApJ...951..111C

Chen, C. H., Li, A., Bohac, C., et al. 2007, The Astrophysical Journal, 666, 466, publisher: IOP Publishing

Collaboration, T. A., Price-Whelan, A. M., Lim, P. L., et al. 2022, The Astropy Project: Sustaining and Growing a Community-oriented Open-source Project and the Latest Major Release (v5.0) of the Core Package, arXiv:2206.14220 [astro-ph]

Combi, M. R. 1996, Icarus, 123, 207, aDS Bibcode: 1996Icar..123..207C

Cronin-Coltsmann, P. F., Kennedy, G. M., Kral, Q., et al. 2023, Monthly Notices of the Royal Astronomical Society, 526, 5401, publisher: OUP ADS Bibcode: 2023MNRAS.526.5401C

Crotts, K. A., Matthews, B. C., Duchêne, G., et al. 2024, The Astrophysical Journal, 961, 245, publisher: IOP ADS Bibcode: 2024ApJ...961..245C

Cutri, R. M., Skrutskie, M. F., van Dyk, S., et al. 2003, VizieR Online Data Catalog, 2246, II/246, aDS Bibcode: 2003yCat.2246...0C

D'Antona, F. & Mazzitelli, I. 1997, Memorie della Società Astronomica Italiana, 68, 807, aDS Bibcode: 1997MmSAI..68..807D

Dent, W. R. F., Greaves, J. S., & Coulson, I. M. 2005, Monthly Notices of the Royal Astronomical Society, 359, 663, publisher: OUP ADS Bibcode: 2005MNRAS.359..663D

Desgrange, C., Milli, J., Chauvin, G., et al. 2025, Astronomy and Astrophysics, 698, A183, publisher: EDP ADS Bibcode: 2025A&A...698A.183D

Dohnanyi, J. S. 1969, Journal of Geophysical Research, 74, 2531, aDS Bibcode: 1969JGR....74.2531D

Dorn, R. J., Bristow, P., Smoker, J. V., et al. 2023, Astronomy and Astrophysics, 671, A24, publisher: EDP ADS Bibcode: 2023A&A...671A..24D

Favre, C., Cleeves, L. I., Bergin, E. A., Qi, C., & Blake, G. A. 2013, The Astrophysical Journal, 776, L38, publisher: IOP ADS Bibcode: 2013ApJ...776L..38F

Feldman, P. D., Weaver, H. A., & Burgh, E. B. 2002, The Astrophysical Journal, 576, L91

Fernandez, R., Wu, Y., & Brandeker, A. 2005, Journal of the Royal Astronomical Society of Canada, 99, 137, aDS Bibcode: 2005JRASC..99S.137F

Flagg, L., Johns-Krull, C. M., France, K., et al. 2021, The Astrophysical Journal, 921, 86, publisher: IOP ADS Bibcode: 2021ApJ...921..86F

Flagg, L., Johns-Krull, C. M., France, K., et al. 2022, The Astrophysical Journal, 934, 8, publisher: IOP ADS Bibcode: 2022ApJ...934....8F

Foreman-Mackey, D., Hogg, D. W., Lang, D., & Goodman, J. 2013, Publications of the Astronomical Society of the Pacific, 125, 306, arXiv:1202.3665 [astro-ph, physics:physics, stat]

Gamache, R. R., Vispoel, B., Rey, M., et al. 2021, Journal of Quantitative Spectroscopy and Radiative Transfer, 271, 107713

Gordon, I. E., Rothman, L. S., Hargreaves, R. J., et al. 2022, Journal of Quantitative Spectroscopy and Radiative Transfer, 277, 107949

Hales, A. S., Marino, S., Sheehan, P. D., et al. 2022, The Astrophysical Journal, 940, 161, publisher: The American Astronomical Society

Heays, A. N., Bosman, A. D., & Dishoeck, E. F. v. 2017, Astronomy & Astrophysics, 602, A105, publisher: EDP Sciences

Higuchi, A. E., Sato, A., Tsukagoshi, T., et al. 2017, The Astrophysical Journal Letters, 839, L14, publisher: The American Astronomical Society

Hobbs, L. M., Vidal-Madjar, A., Ferlet, R., Albert, C. E., & Gry, C. 1985, The Astrophysical Journal, 293, L29, aDS Bibcode: 1985ApJ...293L..29H

Hughes, A. M., Duchêne, G., & Matthews, B. C. 2018, Annual Review of Astronomy and Astrophysics, 56, 541, aDS Bibcode: 2018ARA&A..56..541H

Hughes, A. M., Lieman-Sifry, J., Flaherty, K. M., et al. 2017, The Astrophysical Journal, 839, 86, aDS Bibcode: 2017ApJ...839..86H

Iwasaki, K., Kobayashi, H., Higuchi, A. E., & Aikawa, Y. 2023, The Astrophysical Journal, 950, 36, aDS Bibcode: 2023ApJ...950...36I

Kama, M., Bruderer, S., Dishoeck, E. F. v., et al. 2016, Astronomy & Astrophysics, 592, A83, publisher: EDP Sciences

Klusmeyer, J., Hughes, A. M., Matrà, L., et al. 2021, The Astrophysical Journal, 921, 56, aDS Bibcode: 2021ApJ...921..56K

Kochanov, R. V., Gordon, I. E., Rothman, L. S., et al. 2016, Journal of Quantitative Spectroscopy and Radiative Transfer, 177, 15

Kóspál, Á., Moór, A., Juhász, A., et al. 2013, The Astrophysical Journal, 776, 77, aDS Bibcode: 2013ApJ...776...77K

Kral, Q., Marino, S., Wyatt, M. C., Kama, M., & Matrà, L. 2019, Monthly Notices of the Royal Astronomical Society, 489, 3670, aDS Bibcode: 2019MNRAS.489.3670K

Kral, Q., Matrà, L., Wyatt, M. C., & Kennedy, G. M. 2017, Monthly Notices of the Royal Astronomical Society, 469, 521, aDS Bibcode: 2017MNRAS.469..521K

Kraus, A. L. & Hillenbrand, L. A. 2009, The Astrophysical Journal, 704, 531, publisher: The American Astronomical Society

Krijt, S., Bosman, A. D., Zhang, K., et al. 2020, The Astrophysical Journal, 899, 134, publisher: IOP ADS Bibcode: 2020ApJ...899..134K

Krijt, S., Schwarz, K. R., Bergin, E. A., & Ciesla, F. J. 2018, The Astrophysical Journal, 864, 78, publisher: IOP ADS Bibcode: 2018ApJ...864..78K

Lecavelier des Etangs, A., Vidal-Madjar, A., Roberge, A., et al. 2001, Nature, 412, 706, aDS Bibcode: 2001Natur.412..706L

Lee, R. A., Gaidos, E., van Saders, J., Feiden, G. A., & Gagné, J. 2024, Monthly Notices of the Royal Astronomical Society, 528, 4760, publisher: OUP ADS Bibcode: 2024MNRAS.528.4760L

Leibundgut, B., van den Ancker, M., Courtney-Barrer, B., et al. 2022, The Messenger, 187, 17, aDS Bibcode: 2022Msngr.187...17L

Lieman-Sifry, J., Hughes, A. M., Carpenter, J. M., et al. 2016, The Astrophysical Journal, 828, 25, publisher: IOP ADS Bibcode: 2016ApJ...828..25L

Lisse, C. M., Sitko, M. L., Russell, R. W., et al. 2017, The Astrophysical Journal, 840, L20, publisher: IOP ADS Bibcode: 2017ApJ...840L..20L

Luhman, K. L. & Rieke, G. H. 1999, The Astrophysical Journal, 525, 440, publisher: IOP Publishing

Macías, E., Espaillat, C. C., Ribas, Á., et al. 2018, The Astrophysical Journal, 865, 37, publisher: IOP ADS Bibcode: 2018ApJ...865...37M

Makarov, V. V. 2007, The Astrophysical Journal, 658, 480, publisher: IOP ADS Bibcode: 2007ApJ...658..480M

Mannings, V. & Sargent, A. I. 2000, The Astrophysical Journal, 529, 391, publisher: IOP Publishing

Marino, S., Bonsor, A., Wyatt, M. C., & Kral, Q. 2018, Monthly Notices of the Royal Astronomical Society, 479, 1651

Marino, S., Flock, M., Henning, T., et al. 2020, Monthly Notices of the Royal Astronomical Society, 492, 4409

Marino, S., Matrà, L., Stark, C., et al. 2016, Monthly Notices of the Royal Astronomical Society, 460, 2933, publisher: OUP ADS Bibcode: 2016MNRAS.460.2933M

Matrà, L., Dent, W. R. F., Wyatt, M. C., et al. 2017a, Monthly Notices of the Royal Astronomical Society, 464, 1415, publisher: OUP ADS Bibcode: 2017MNRAS.464.1415M

Matrà, L., MacGregor, M. A., Kalas, P., et al. 2017b, The Astrophysical Journal, 842, 9, aDS Bibcode: 2017ApJ...842...9M

Matrà, L., Marino, S., Kennedy, G. M., et al. 2018a, The Astrophysical Journal, 859, 72, publisher: The American Astronomical Society

Matrà, L., Marino, S., Wilner, D. J., et al. 2025, Astronomy and Astrophysics, 693, A151, publisher: EDP ADS Bibcode: 2025A&A...693A.151M

Matrà, L., Öberg, K. I., Wilner, D. J., Olofsson, J., & Bayo, A. 2019, The Astronomical Journal, 157, 117, publisher: The American Astronomical Society

Matrà, L., Wilner, D. J., Öberg, K. I., et al. 2018b, The Astrophysical Journal, 853, 147, aDS Bibcode: 2018ApJ...853..147M

Mawet, D., Absil, O., Montagnier, G., et al. 2012, Astronomy & Astrophysics, 544, A131, publisher: EDP Sciences

McClure, M. K., Bergin, E. A., Cleeves, L. I., et al. 2016, The Astrophysical Journal, 831, 167, publisher: The American Astronomical Society

Melis, C., Zuckerman, B., Rhee, J. H., et al. 2013, The Astrophysical Journal, 778, 12, arXiv:1308.2753 [astro-ph]

Merín, B., Montesinos, B., Eiroa, C., et al. 2004, Astronomy and Astrophysics, 419, 301, publisher: EDP ADS Bibcode: 2004A&A...419..301M

Moór, A., Curé, M., Kóspál, Á., et al. 2017, The Astrophysical Journal, 849, 123, aDS Bibcode: 2017ApJ...849..123M

Moór, A., Kóspál, Á., Ábrahám, P., & Pawellek, N. 2020, 345, 349, conference Name: Origins: From the Protosun to the First Steps of Life ADS Bibcode: 2020IAUS..345..349M

Morbidelli, A., Lunine, J., O'Brien, D., Raymond, S., & Walsh, K. 2012, Annual Review of Earth and Planetary Sciences, 40, 251, \_eprint: <https://doi.org/10.1146/annurev-earth-042711-105319>

Müller, A., van den Ancker, M. E., Launhardt, R., et al. 2011, Astronomy and Astrophysics, 530, A85, publisher: EDP ADS Bibcode: 2011A&A...530A..85M

Nakatani, R., Turner, N. J., Hasegawa, Y., et al. 2023, The Astrophysical Journal, 959, L28, aDS Bibcode: 2023ApJ...959L..28N

Natta, A., Testi, L., & Randich, S. 2006, Astronomy and Astrophysics, 452, 245, publisher: EDP ADS Bibcode: 2006A&A...452..245N

Neuhäuser, R., Walter, F. M., Covino, E., et al. 2000, Astronomy and Astrophysics Supplement Series, 146, 323, number: 2 Publisher: EDP Sciences

Pannier, E. & Laux, C. O. 2019, Journal of Quantitative Spectroscopy and Radiative Transfer, 222-223, 12

Pearce, T. D. 2024, Debris disks around main-sequence stars, publication Title: arXiv e-prints ADS Bibcode: 2024arXiv240311804P

Pecaut, M. J., Mamajek, E. E., & Bubar, E. J. 2012, The Astrophysical Journal, 746, 154, publisher: IOP ADS Bibcode: 2012ApJ...746..154P

Pineda, J. E., Szulágyi, J., Quanz, S. P., et al. 2019, The Astrophysical Journal, 871, 48, publisher: The American Astronomical Society

Quéméner, G. & Balakrishnan, N. 2009, The Journal of Chemical Physics, 130, 114303

Rebolledo, I., Ribas, Á., de Gregorio-Monsalvo, I., et al. 2022, Monthly Notices of the Royal Astronomical Society, 509, 693, publisher: OUP ADS Bibcode: 2022MNRAS.509..693R

Rhee, J. H., Song, I., Zuckerman, B., & McElwain, M. 2007, The Astrophysical Journal, 660, 1556, arXiv:astro-ph/0609555

Riviere-Marichalar, P., Barrado, D., Montesinos, B., et al. 2014, Astronomy and Astrophysics, 565, A68, publisher: EDP ADS Bibcode: 2014A&A...565A..68R

Roberge, A., Feldman, P. D., Lagrange, A. M., et al. 2000, The Astrophysical Journal, 538, 904, aDS Bibcode: 2000ApJ...538..904R

Robitaille, T. P., Whitney, B. A., Indebetouw, R., & Wood, K. 2007, The Astrophysical Journal Supplement Series, 169, 328, publisher: IOP Publishing

Schneider, P. C., Manara, C. F., Faccinini, S., et al. 2018, Astronomy & Astrophysics, 614, A108, publisher: EDP Sciences

Schwarz, K. R., Bergin, E. A., Cleeves, L. I., et al. 2016, The Astrophysical Journal, 823, 91, publisher: The American Astronomical Society

Schwarz, K. R., Bergin, E. A., Cleeves, L. I., et al. 2018, The Astrophysical Journal, 856, 85, publisher: IOP ADS Bibcode: 2018ApJ...856..85S

Siess, L., Dufour, E., & Forestini, M. 2000, An internet server for pre-main sequence tracks of low- and intermediate-mass stars, iSSN: 0004-6361 Volume: 358 ADS Bibcode: 2000A&A...358..593S

Simon, M., Dutrey, A., & Guilloteau, S. 2000, The Astrophysical Journal, 545, 1034, publisher: IOP ADS Bibcode: 2000ApJ...545.1034S

Smette, A., Sana, H., Noll, S., et al. 2015, Astronomy & Astrophysics, 576, A77, arXiv:1501.07239 [astro-ph]

Smirnov-Pinchukov, G. V., Moór, A., Semenov, D. A., et al. 2022, Monthly Notices of the Royal Astronomical Society, 510, 1148, aDS Bibcode: 2022MNRAS.510.1148S

Thi, W. F., Kamp, I., Woitke, P., et al. 2013, Astronomy and Astrophysics, 551, A49, publisher: EDP ADS Bibcode: 2013A&A...551A..49T

Torres, C. A. O., Quast, G. R., Melo, C. H. F., & Sterzik, M. F. 2008, in Handbook of Star Forming Regions, Volume II, Vol. 5, 757, aDS Bibcode: 2008hsf2.book..757T

Trapman, L., Longarini, C., Rosotti, G. P., et al. 2025, The Astrophysical Journal, 984, L18, publisher: IOP ADS Bibcode: 2025ApJ...984L..18T

Trapman, L., Miotello, A., Kama, M., van Dishoeck, E. F., & Bruderer, S. 2017, Astronomy and Astrophysics, 605, A69, aDS Bibcode: 2017A&A...605A..69T

Troutman, M. R., Hinkle, K. H., Najita, J. R., Rettig, T. W., & Brittain, S. D. 2011, The Astrophysical Journal, 738, 12, aDS Bibcode: 2011ApJ...738...12T

Ulmer-Moll, S., Figueira, P., Neal, J. J., Santos, N. C., & Bonnefoy, M. 2019, Astronomy and Astrophysics, 621, A79, aDS Bibcode: 2019A&A...621A..79U

Vióque, M., Oudmaijer, R. D., Baines, D., Mendigutía, I., & Pérez-Martínez, R. 2018, Astronomy & Astrophysics, 620, A128, publisher: EDP Sciences

Visser, R., Van Dishoeck, E. F., & Black, J. H. 2009, Astronomy & Astrophysics, 503, 323

Wichittanakom, C., Oudmaijer, R. D., Fairlamb, J. R., et al. 2020, Monthly Notices of the Royal Astronomical Society, 493, 234

Worthen, K., Chen, C. H., Brittain, S. D., et al. 2024, The Astrophysical Journal, 962, 166, aDS Bibcode: 2024ApJ...962..166W

Wyatt, M. 2020, Extrasolar Kuiper belts, pages: 351-376 Publication Title: The Trans-Neptunian Solar System ADS Bibcode: 2020tnss.book..351W

Zaire, B., Donati, J. F., Alencar, S. P., et al. 2024, Monthly Notices of the Royal Astronomical Society, 533, 2893, publisher: OUP ADS Bibcode: 2024MN-RAS.533.2893Z

Zhang, K., Bergin, E. A., Blake, G. A., Cleeves, L. I., & Schwarz, K. R. 2017, Nature Astronomy, 1, 1, publisher: Nature Publishing Group

Zhang, K., Bergin, E. A., Schwarz, K., Krijt, S., & Ciesla, F. 2019, The Astrophysical Journal, 883, 98, publisher: The American Astronomical Society

Zhang, K., Schwarz, K. R., & Bergin, E. A. 2020, The Astrophysical Journal, 891, L17, publisher: IOP ADS Bibcode: 2020ApJ..891L..17Z

Zuckerman, B. & Song, I. 2012, The Astrophysical Journal, 758, 77, aDS Bibcode: 2012ApJ...758...77Z

Zuckerman, B. M. 1995, NSF Award, 94, 17158, aDS Bibcode: 1995nsf....9417158Z

## Appendix A: Molecfit Telluric Corrections

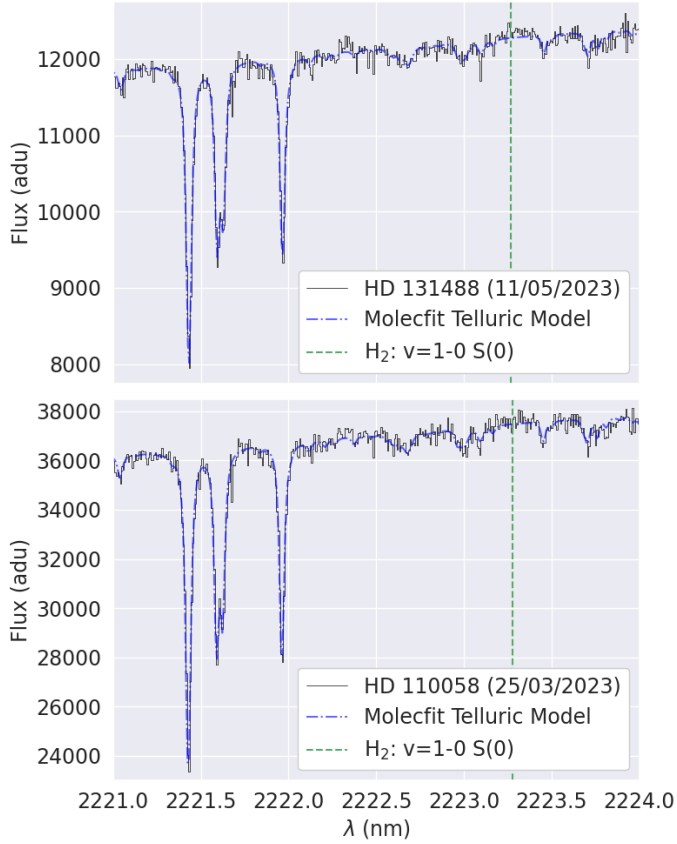


Fig. A.1: CRIRES+ spectra of HD 131488 and HD 110058 near the H<sub>2</sub> v=1-0 S(0) line (black lines). In blue is the best-fit atmospheric transmission model from molecfit consisting of CH<sub>4</sub> and H<sub>2</sub>O absorption lines, combined with our (linear) best-fit continuum model. The vertical green line denotes the expected location of the H<sub>2</sub> transition of interest.

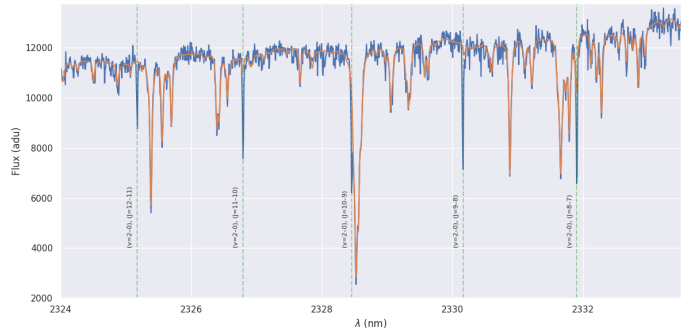


Fig. A.2: A portion of an example spectrum (blue) overlaid with the telluric fit (orange) produced by molecfit over the data from a single nodding position/day combination (the combined nodding A frames on the night of 08/03/2024). The locations of <sup>12</sup>CO lines are marked with green dashed lines.

## Appendix B: On CRIRES+ wavelength calibration offset between nodding positions

Our observations are taken with the 0.2" width slit on CRIRES. When reducing our data, the ESO data reduction pipeline re-

ported that for both of our targets, the width of the slit was not fully illuminated. This has two consequences for our observations detailed in the ESO CR2RES pipeline user manual in the known issues section 7.1 on "Superresolution". Relevant to this study, this gives us increased resolution but at the cost of the default wavelength solution produced by the ESO pipeline being unreliable between nodding frames. To account for this, we take the combined spectra for each nodding position and separately feed each one through molecfit to acquire a final wavelength solution fit to the tellurics in the data. For each star this means we fit 8 spectra for <sup>12</sup>CO (2 days, 2 nodding positions, and 2 sub-orders) and 4 spectra for H<sub>2</sub> (2 days and 2 nodding positions). When presenting the results in this paper, we show plots of the median of these spectra. Any combination or modelling of spectra with an incorrect wavelength solution would distort the line shapes and positions, diminishing the accuracy of our results. The degree to which this is an issue is shown in Figures B.1 and B.2 which show the pre-corrected wavelength solution can err by as much as a pixel. The higher post-correction correlation in Figure B.2 demonstrates numerically that the alignment of the spectra is improved.

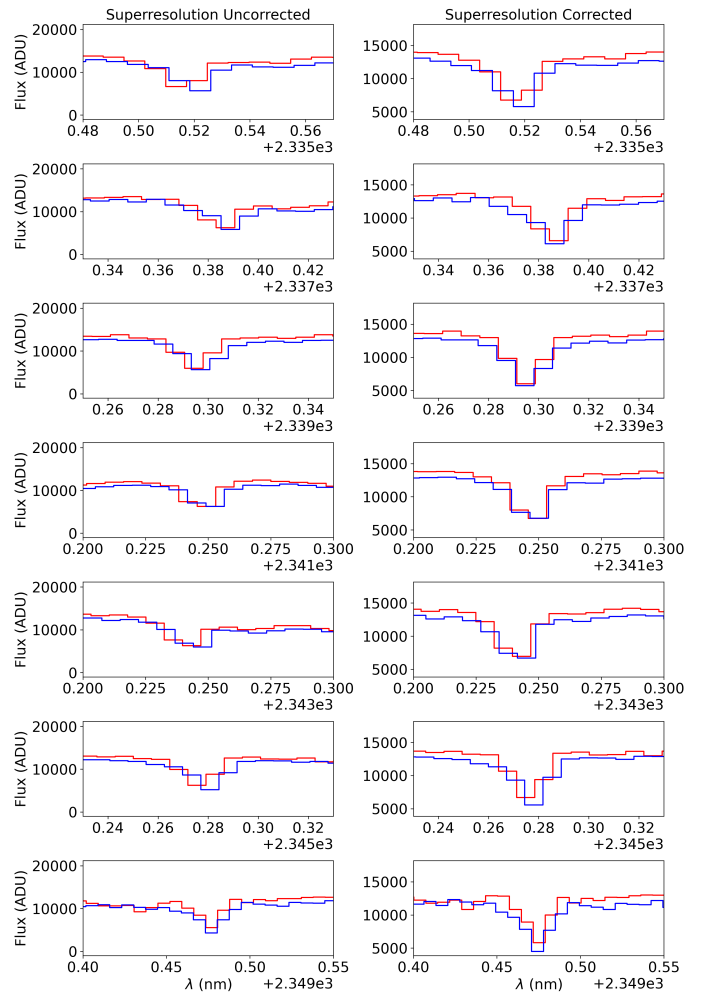


Fig. B.1: <sup>12</sup>CO lines before and after superresolution correction. In red, the nodding A frames should align with the nodding B frames as these observations were taken on the same day if the wavelength solution is accurate.

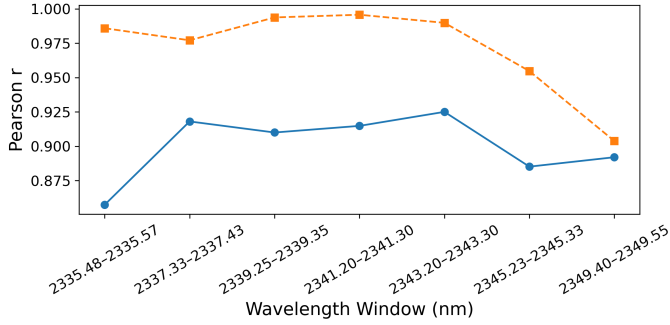
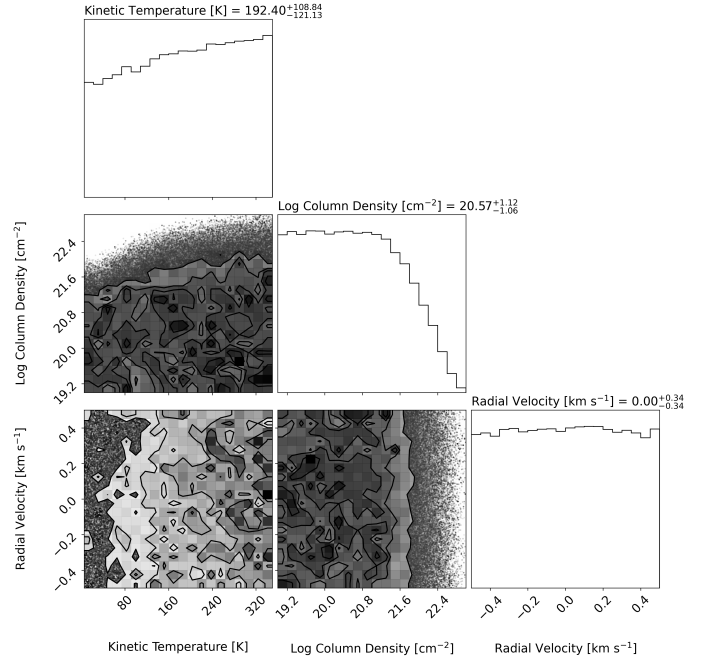


Fig. B.2: Pearson correlations of the uncorrected (blue) and post-correction (orange)  $^{12}\text{CO}$  lines from Figure B.1.



### Appendix C: MCMC Posterior Distributions

In Figures C.1, and C.2 we show the posterior distributions from the MCMC simulations for  $\text{H}_2$ . Given that  $\text{H}_2$  is not detected in either system, the 2d corner plots show upper limits for the  $\text{H}_2$  column density and unconstrained temperature as expected for a non-detection. Higher temperatures allow for larger column densities as the thermal broadening produces shallower, wider lines which are more difficult to detect than the narrower, deeper lines produced by cold gas.

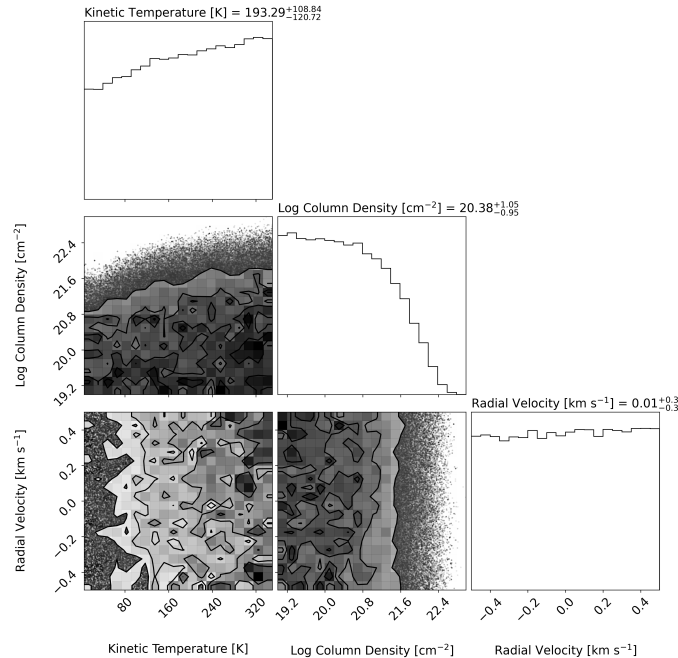
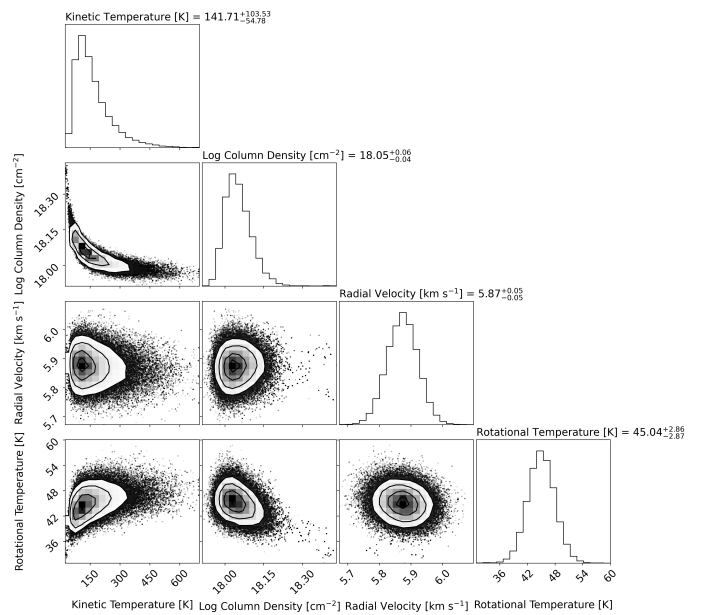


Fig. C.1: Posterior probability distributions of excitation temperature and column density from the 2223.29 nm rovibrational  $\text{H}_2$  absorption model fit to the HD 131488 data. Marginalised distributions for each parameter are displayed on the diagonal.

Fig. C.2: Posterior probability distributions of excitation temperature and column density from the 2223.29 nm rovibrational  $\text{H}_2$  absorption model fit to the HD 110058 data. Marginalised distributions for each parameter are displayed on the diagonal.



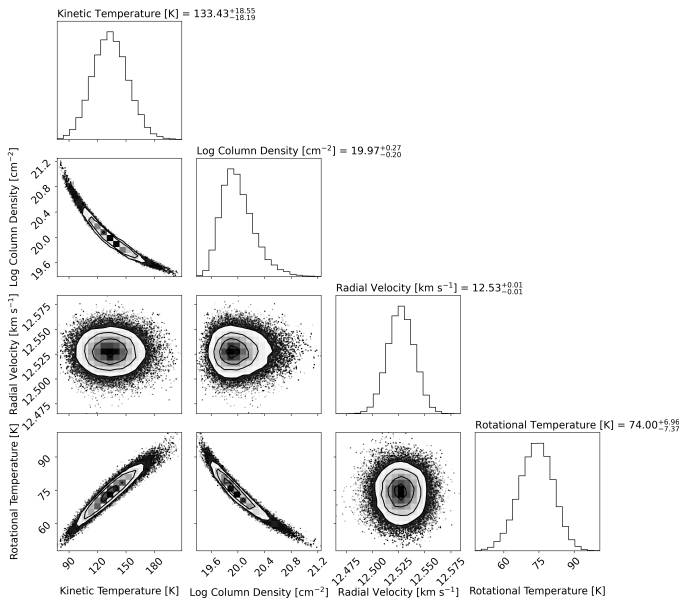


Fig. C.4: Posterior probability distributions of excitation temperature, kinetic temperature, radial velocity, and column density from the for the  $^{12}\text{CO}$  absorption model fit to the HD 110058 data. Marginalised distributions for each parameter are displayed on the diagonal.

#### Appendix D: CO/H<sub>2</sub> Ratios for Protoplanetary and Exocometary Belt Gas

The determination of the ages and gas masses of protoplanetary disks is difficult and an active area of research (Zhang et al. 2020). A variety of techniques have been used to determine the gas mass including assuming a gas-to-dust ratio, and assuming ISM-like CO isotopologue ratios to give estimates of the mass of the typically optically thick  $^{12}\text{CO}$  in disks. The amount of H<sub>2</sub> can be estimated from assuming ISM-like HD to H<sub>2</sub> ratios, dust-to-gas ratios, gas/dust kinematics, or through N<sub>2</sub>H<sup>+</sup>.

Table D.1: CO to H<sub>2</sub> Ratios and Age for Disks

Name	CO/H <sub>2</sub> Ratio	Age (Myr)	CO Method	H <sub>2</sub> Method	Age Method	Type	References
ISM	-4.00	—	—	—	—	ISM	—
HL Tau	-4.17 <sup>+0.04</sup> <sub>-0.03</sub>	0.8 <sup>+0.25</sup> <sub>-0.25</sub>	<sup>13</sup> CO	Dust	SED	PPD	[1,2]
DG Tau	-4.34 <sup>+0.04</sup> <sub>-0.04</sub>	0.9 <sup>+0.25</sup> <sub>-0.25</sub>	<sup>13</sup> CO	Dust	SED	PPD	[1,2]
TMC1A	-3.68 <sup>+0.02</sup> <sub>-0.04</sub>	0.5 <sup>+0.1</sup> <sub>-0.1</sub>	<sup>13</sup> CO	Dust	SED	PPD	[1,2]
Oph-IRS67	-3.68 <sup>+0.30</sup> <sub>-0.30</sub>	0.45 <sup>+0.1</sup> <sub>-0.1</sub>	C <sup>17</sup> O	Dust	SED	PPD	[3,2]
DM Tau	-4.24 <sup>+0.15</sup> <sub>-0.21</sub>	1.5 <sup>+0.8</sup> <sub>-0.25</sub>	<sup>13</sup> CO, C <sup>18</sup> O	N <sub>2</sub> H <sup>+</sup>	SED	PPD	[2,4,30]
TW Hya	-5.84 <sup>+0.00</sup> <sub>-0.30</sub>	8 <sup>+1</sup> <sub>-1</sub>	<sup>13</sup> CO, C <sup>18</sup> O	Dust	TW Hydra	PPD	[4,28]
HD163296	-4.28 <sup>+0.17</sup> <sub>-0.21</sub>	6.03 <sup>+0.28</sup> <sub>-0.27</sub>	<sup>13</sup> CO, C <sup>18</sup> O	N <sub>2</sub> H <sup>+</sup>	Isochrones	PPD	[4,5,30]
IM Lup	-4.45 <sup>+0.21</sup> <sub>-0.20</sub>	1.2 <sup>+0.8</sup> <sub>-0.25</sub>	<sup>13</sup> CO, C <sup>18</sup> O	N <sub>2</sub> H <sup>+</sup>	Isochrones	PPD	[4,29,30]
J1609 J1608	< -6.00	8 <sup>+3</sup> <sub>-3</sub>	C <sup>18</sup> O	N <sub>2</sub> H <sup>+</sup>	Upper Sco	PPD	[6,30]
HD100546	-4.70 <sup>+0.30</sup> <sub>-0.30</sub>	4.8 <sup>+2</sup> <sub>-1</sub>	<sup>12</sup> CO, <sup>13</sup> CO, C <sup>18</sup> O	HD	Isochrones	PPD	[7,8,9,31]
PDS 66	-5.53 <sup>+0.28</sup> <sub>-0.29</sub>	3.1 <sup>+0.9</sup> <sub>-0.9</sub>	<sup>13</sup> CO, C <sup>18</sup> O	N <sub>2</sub> H <sup>+</sup>	Isochrones	PPD	[10,30,32]
AA Tau	-4.60 <sup>+0.24</sup> <sub>-0.22</sub>	7	<sup>13</sup> CO, C <sup>18</sup> O	N <sub>2</sub> H <sup>+</sup>	Isochrones	PPD	[11,30,32]
AS 209	-4.68 <sup>+0.25</sup> <sub>-0.26</sub>	0.75 <sup>+0.25</sup> <sub>-0.25</sub>	<sup>13</sup> CO, C <sup>18</sup> O	N <sub>2</sub> H <sup>+</sup>	$\rho$ Ophiuchi	PPD	[12,30, 33]
CQ Tau	-4.50 <sup>+0.30</sup> <sub>-0.08</sub>	10.0	<sup>13</sup> CO, C <sup>18</sup> O	N <sub>2</sub> H <sup>+</sup>	Isochrones	PPD	[13,30]
Elias 2-27	-4.20 <sup>+0.14</sup> <sub>-0.19</sub>	0.8	<sup>13</sup> CO, C <sup>18</sup> O	N <sub>2</sub> H <sup>+</sup>	$\rho$ Orph	PPD	[14,30,34]
GM Aur	-4.38 <sup>+0.21</sup> <sub>-0.23</sub>	6.5 <sup>+3.5</sup> <sub>-3.5</sub>	<sup>13</sup> CO, C <sup>18</sup> O	N <sub>2</sub> H <sup>+</sup>	Isochrones	PPD	[15,30,35]
HD 135344B	-4.13 <sup>+0.10</sup> <sub>-0.17</sub>	9.0 <sup>+2.0</sup> <sub>-2.0</sub>	<sup>13</sup> CO, C <sup>18</sup> O	N <sub>2</sub> H <sup>+</sup>	Isochrones	PPD	[16,30]
HD 143006	-5.11 <sup>+0.25</sup> <sub>-0.23</sub>	8.0 <sup>+4.0</sup> <sub>-4.0</sub>	<sup>13</sup> CO, C <sup>18</sup> O	N <sub>2</sub> H <sup>+</sup>	Upper Sco	PPD	[17,30]
HD 34282	-4.11 <sup>+0.07</sup> <sub>-0.12</sub>	6.4 <sup>+0.5</sup> <sub>-0.5</sub>	<sup>13</sup> CO, C <sup>18</sup> O	N <sub>2</sub> H <sup>+</sup>	Isochrones	PPD	[18,30]
LkCa 15	-4.46 <sup>+0.20</sup> <sub>-0.21</sub>	2.0 <sup>+2.0</sup> <sub>-1.0</sub>	<sup>13</sup> CO, C <sup>18</sup> O	N <sub>2</sub> H <sup>+</sup>	Isochrones	PPD	[19,30]
HD 31648	-4.22 <sup>+0.15</sup> <sub>-0.21</sub>	6.55 <sup>+0.55</sup> <sub>-0.55</sub>	<sup>13</sup> CO, C <sup>18</sup> O	N <sub>2</sub> H <sup>+</sup>	Isochrones	PPD	[20,30]
HD 36112	-4.25 <sup>+0.15</sup> <sub>-0.21</sub>	8.5 <sup>+0.4</sup> <sub>-0.5</sub>	<sup>13</sup> CO, C <sup>18</sup> O	N <sub>2</sub> H <sup>+</sup>	Isochrones	PPD	[21,30]
RXJ 1615.3-3255	-4.12 <sup>+0.08</sup> <sub>-0.12</sub>	1.0	<sup>13</sup> CO, C <sup>18</sup> O	N <sub>2</sub> H <sup>+</sup>	Lupus	PPD	[22,30]
RXJ 1842.9-3532	-4.60 <sup>+0.22</sup> <sub>-0.22</sub>	10.0	<sup>13</sup> CO, C <sup>18</sup> O	N <sub>2</sub> H <sup>+</sup>	Isochrones	PPD	[23,30]
V4046 Sgr	-4.60 <sup>+0.20</sup> <sub>-0.21</sub>	12.0	<sup>13</sup> CO, C <sup>18</sup> O	N <sub>2</sub> H <sup>+</sup>	Isochrones	PPD	[24,30]
HD 131488	> -4.66	16 <sup>+2</sup> <sub>-2</sub>	<sup>12</sup> CO	H <sub>2</sub>	Upper Centaurus Lupus	Debris Disk	[25,26]
HD 110058	> -2.45	17 <sup>+3</sup> <sub>-3</sub>	<sup>12</sup> CO	H <sub>2</sub>	Lower Centaurus Crux	Debris Disk	[25,27]
Beta Pictoris	> -3.19	23 <sup>+8</sup> <sub>-8</sub>	<sup>12</sup> CO	H <sub>2</sub>	$\beta$ Pictoris	Debris Disk	[36,37]

**References.** (1) Zhang et al. (2020); (2) Robitaille et al. (2007); (3) Artur de la Villarmois et al. (2018); (4) Zhang et al. (2019); (5) Wichitanakom et al. (2020); (6) Anderson et al. (2019); (7) Kama et al. (2016); (8) Bruderer et al. (2012); (9) Pineda et al. (2019); (10) Asensio-Torres et al. (2021); (11) Schneider et al. (2018); (12) Natta et al. (2006); (13) Mannings & Sargent (2000); (14) Andrews et al. (2009); (15) Macías et al. (2018); (16) Müller et al. (2011); (17) Pecaut et al. (2012); (18) Merín et al. (2004); (19) Kraus & Hillenbrand (2009); (20) Simon et al. (2000); (21) Vioque et al. (2018); (22) Makarov (2007); (23) Neuhäuser et al. (2000); (24) Torres et al. (2008); (25) This work; (26) Pecaut et al. (2012); (27) Pecaut et al. (2012); (28) Rhee et al. (2007); (29) Mawet et al. (2012); (30) Trapman et al. (2025); (31) Bergin & Williams (2018); (32) Siess et al. (2000); (33) D'Antona & Mazzitelli (1997); (34) Luhman & Rieke (1999), (35) Zaire et al. (2024) (36) Lee et al. (2024); (37) Lecavelier des Etangs et al. (2001)